Journal of Medicinal Chemistry

ARTICLE

pubs.acs.org/jmc

# Design, Synthesis, and Evaluation of Coumarin-Based Molecular Probes for Imaging of Myelination

Changning Wang,[†] Chunying Wu,[†] Junqing Zhu,[†] Robert H. Miller,[‡] and Yanming Wang*[,†]

[†]Division of Radiopharmaceutical Science, Case Center for Imaging Research, Department of Radiology, Case Western Reserve University, Cleveland, Ohio 44106, United States

[‡]Department of Neurosciences, Case Western Reserve University, Cleveland, Ohio 44106, United States

Supporting Information

**ABSTRACT:** Myelination represents one of the most fundamental biological processes in the vertebrate nervous system. Abnormalities and changes in myelination in the central nervous system (CNS) are seen in many neurodegenerative disorders, such as multiple sclerosis (MS). A long-standing goal has been to directly detect and quantify myelin content in order to facilitate diagnosis and therapeutic treatments of myelin-related diseases. In the course of our studies, we have developed a series of small-molecule probes (SMP) as myelin-imaging agents. Among them are coumarin derivatives, which exhibit promising brain permeability and myelin-binding properties. Herein we report a full account of the design and synthesis of coumarin-based SMPs as myelin-imaging agents. Systematic evaluation of these SMPs in both the CNS and peripheral nervous system (PNS) allowed us to identify some lead agents for potential use as fluorescent dyes for intraoperative nerve mapping in surgical operations or as radiotracers for positron emission tomography (PET) imaging of myelination.


## INTRODUCTION

Multiple sclerosis (MS) is the most commonly acquired demyelinating disease in humans, currently affecting 350,000 Americans and 2 million people worldwide.[1] MS is characteristic of myelin loss in the central nervous system, leading to axonal damage.[2−5] In order to restore new myelin sheaths to demyelinated regions to protect axons, efforts have been made to promote endogenous repair mechanisms and/or transplant an exogenous source of myelinating cells to the demyelinated regions.[6−12] To achieve this goal, significant progress has been made and several clinical trials are currently being conducted.[13,14]

A major challenge in such clinical studies has been the need to assess and quantify any changes in myelin content *in vivo*. To date, magnetic resonance imaging (MRI) has been used as the primary tool for detection of brain lesions in MS.[15] However, MRI cannot distinguish lesions caused by demyelination or inflammation, which often coexist in the brain. This is due to the fact that any changes in signal intensity on a dual echo T2-weighted sequence are based on tissue water content. As a result, the use of MRI as a primary outcome measure of MS disease activity has been shown to be uncorrelated with clinical outcomes.[16] For this reason, we set out to develop small-molecule probes (SMP) that bind to myelin membranes with high affinity and specificity. Over the past years, we have developed a series of SMPs that readily penetrate the blood−brain barrier and selectively bind to myelin with high affinity and specificity[17−22] (Figure 1). Compared to conventional myelin stains such as luxol fast blue and fluoromyelin, these molecular probes are capable of direct imaging of myelination *in vivo*. For example, some of these SMPs have been used for positron emission tomography (PET), which is widely used to study biochemical and metabolic changes at the molecular level.[17,20] One of the lead myelin-imaging agents has also been used for myelin imaging in nonhuman primates.[17]

In the course of our studies, we have focused our efforts on the design and synthesis of a series of coumarin derivatives as myelin-imaging agents[23] (Table 1). Coumarin is a natural product occurring in plants and has many important biological activities.[24,25] We have previously reported a coumarin derivative, 3-(4-aminophenyl)-2*H*-chromen-2-one, termed CMC, which exhibits promising myelin-binding properties.[23] To fully examine the potential of this class of compounds as myelin-imaging agents, we evaluated 36 coumarin derivatives through *in vitro* fluorescent tissue staining and *in vivo* fluorescent imaging. Herein we report a full account of structure−activity studies of these coumarin-based agents, which allow us to identify some lead compounds suitable for myelin imaging in clinically relevant settings.

**Received:** November 19, 2010
**Published:** March 10, 2011

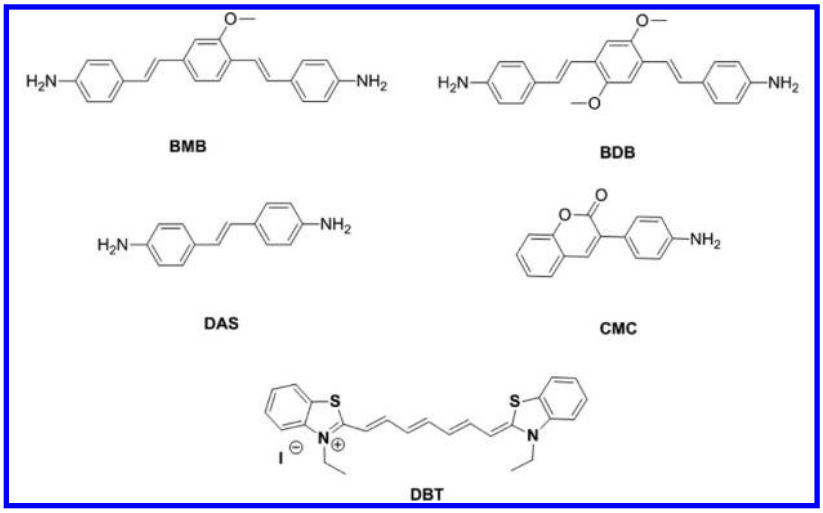


**Figure 1.** Myelin-imaging agents for *in vivo* imaging studies. BMB, BDB, and DAS were precursors of PET-imaging radiotracers. DBT was a novel myelin-specific optical imaging probe. BMB, (*E*,*E*)-1,4-bis(*p*-aminostyryl)-2-methoxybenzene; BDB, (*E*,*E*)-1,4-bis(4′-aminostyryl)-2,5-dimethoxybenzene; DAS, 4,4′-diamino-*trans*-stilbene; CMC, 3-(4-aminophenyl)-2*H*-chromen-2-one; DBT, 3,3′-diethylthiatricarbocyanine iodide.

## RESULTS

**Chemical Synthesis.** Synthesis of some coumarin derivatives (**3**, **18**, **19**, **29**−**36**) was achieved through reactions as shown in Scheme 1. Briefly, substituted salicaldehyde (**37**, **39**, and **40**) and arylacetic acid (**38** and **41**) were reacted with sodium acetate to yield the corresponding coumarin derivatives **3**, **18**, **29**, and **33**. The acetyl groups in **29** and **33** were removed in acidic solution to obtain **30** and **34** and then coupled with side chains to obtain final products **31**, **32**, **35**, and **36**. Further reduction of **3** with $SnCl_2$ in ethanol yielded compound **19**.

**Compound Screening.** All of these compounds are fluorescent, which allowed us to examine their myelin-binding properties by fluorescent microscopy. Thus, **1**−**36** were screened for binding specificity for myelin by histological staining of mouse brain tissue sections. At a concentration of 100 $\mu$M of each compound, whole mouse brain tissue sections containing the white matter and gray matter were incubated for 20 min. The myelin-binding specificity was quantitatively examined by fluorescent intensity in different brain regions.

Based on the fluorescent tissue staining and fluorescent intensity in the predefined region of the corpus callosum, **1**−**36** can be divided into three groups: (1) compounds including **1**−**17**, which showed no binding to compact myelin; (2) **18**−**26**, which showed moderate binding to myelin; and (3) **27**−**36**, which showed high binding. We then further calculated the fluorescence intensity ratio between the white matter and gray matter using predefined regions of interest (ROI) as shown in Figure 2A.

The structure−binding relationship studies led us to propose some molecular based generalities on myelin-binding properties: (1) an aniline moiety in the $R_6$ position is normally necessary for the compound to bind to myelin. The amino group of the aniline moiety can bear methyl, ethyl, or other small alkyl groups (**27**−**36**), but the myelin-binding property is diminished or even lost once the amino group is removed or substituted by a nitro group (**1**−**17**), which suggests that binding takes place through direct interaction of the amino group with myelin membranes; (2) an aniline moiety in the $R_2$ position, such as **20**−**26**, shows only moderate binding to myelin, which indicates that binding interaction is dependent on the geometry of the aniline moiety; (3) substituents in the $R_2$ and $R_3$ positions can be switched without affecting the binding properties; and (4) with the fluoralkyl side chains, the substituents on $R_2$ show higher binding selectivity than on $R_3$.

In addition to the lipophilicity (LogPoct), the fluorescent intensity ratios between the white matter and gray matter of those myelin-binding compounds were also determined as a parameter to quantitatively evaluate the binding specificity. Based on these structure−activity relationship studies, particularly the binding ratios between the white matter and gray matter, **32** stands out with the highest binding specificity for myelin. Thus, we selected **32** (termed FIC) as the lead compound for further studies.

**32 Binds to Myelin in Both the CNS and PNS.** The myelin-binding properties of **32** were further evaluated in both the CNS and PNS through *in vitro* fluorescent staining. Both myelinated corpus callosum and cerebellar regions in CNS and sciatic nerve in PNS were then examined by fluorescent microscopy. At 100 $\mu$M concentration, **32** selectively labeled corpus callosum (Figure 3A) and cerebellum (Figure 3C) in the CNS as well as the sciatic nerves in the PNS (Figure 3E). The **32** staining patterns were found to be virtually identical to the patterns observed in immunohistochemical staining for MBP (Figure 3B and D) or Black-Gold II staining (Figure 3F).

Quantitative analysis indicated that the fluorescent intensity is proportional to the level of myelination present in wild-type (Figure 4A and C) and shiverer mouse (Figure 4B and D) brains. As shown in Figure 4E and F, the MBP antibody staining showed a fluorescent intensity of shiverer mouse brain which is only 14% of that detected in the wild-type control brains. Consistently, **32** staining also exhibited similar fluorescent intensity, which is proportional to the level of myelination. In the shiverer mouse brains, the fluorescent intensity of **32** was 12% of that detected in the wild-type mouse brains, which was consistent with MBP immunostaining.

**32 Stains Myelinated CNS Regions *In Situ*.** Following *in vitro* tissue staining, we then evaluated the brain permeability and subsequent myelin-binding properties of **32** in mice. A dose of **32** (40 mg/kg) was administered to wild-type mice via tail vein

**Table 1. Coumarin-Based Compound Library for Screening of Myelin-Imaging Probes**

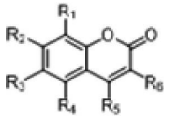

| Entry | $R_1$ | $R_2$ | $R_3$ | $R_4$ | $R_5$ | $R_6$ | Molecular Weight | Log P | Binding |
|---|---|---|---|---|---|---|---|---|---|
| 1 (Coumarin) | H | H | H | H | H | H | 146.14 | 1.82 | - |
| 2 | H | H | H | H | H |  | 267.24 | 3.00 | - |
| 3 | H | H | F | H | H |  | 285.23 | 3.13 | - |
| 4 | H | -$CH_3$ | H | H | H | H | 160.17 | 2.31 | - |
| 5 | H | H | H | H | -$CH_3$ | H | 160.17 | 2.00 | - |
| 6 | H | H | H | H | -$NH_2$ | H | 161.16 | 0.78 | - |
| 7 | H | H | H | H | H | -$NH_2$ | 161.16 | 0.28 | - |
| 8 | H | H | H | H | -OH | H | 162.14 | 1.17 | - |
| 9 | H | H | H | H | H | -OH | 162.14 | 0.66 | - |
| 10 | H | -$OCH_3$ | H | H | H | H | 176.17 | 1.70 | - |
| 11 | H | H | H | H | H |  | 222.24 | 3.36 | - |
| 12 | H | -OH | H | H | H |  | 238.24 | 2.97 | - |
| 13 | H | -$NH_2$ | H | H | -$CH_3$ | H | 175.18 | 1.20 | - |
| 14 | H | -$NH_2$ | H | H | -$CF_3$ | H | 229.16 | 1.63 | - |
| 15 | H | -OH | H | H | -$CF_3$ | H | 230.14 | 2.05 | - |
| 16 | H |  | H | H | -$CF_3$ | H | 257.21 | 2.72 | - |
| 17 | H | H | H | H | -OH |  | 336.29 | 2.12 | - |
| 18 | H | H | F | H | H |  | 283.30 | 3.81 | + |
| 19 | H | H | F | H | H |  | 255.24 | 2.72 | + |
| 20 | H | 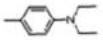 | H | H | H |  | 414.45 | 5.45 | + |
| 21 | H | 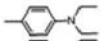 | H | H | H |  | 384.47 | 5.2 | + |
| 22 | H | 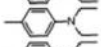 | H | H | H |  | 462.38 | 6.77 | + |
| 23 | H | 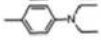 | H | H | H |  | 426.53 | 6.86 | + |
| 24 | H | 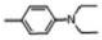 | H | H | H |  | 409.48 | 5.43 | + |
| 25 | H | 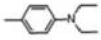 | H | H | H |  | 423.51 | 5.66 | + |
| 26 | H | 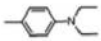 | H | H | H |  | 403.49 | 5.52 | + |
| 27 | H | H | H | H | H |  | 237.25 | 2.70 | ++ |
| 28 | H | H | H | H | H |  | 265.31 | 3.61 | ++ |
| 29 | H | -OAc | H | H | H |  | 323.34 | 3.45 | ++ |
| 30 | H | -OH | H | H | H |  | 281.31 | 3.22 | ++ |
| 31 | H | 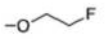 | H | H | H |  | 327.35 | 3.71 | ++ |
| 32 | H |  | H | H | H |  | 341.38 | 3.82 | ++ |
| 33 | H | H | -OAc | H | H |  | 323.34 | 3.23 | ++ |
| 34 | H | H | -OH | H | H |  | 281.31 | 3.26 | ++ |
| 35 | H | H | 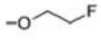 | H | H |  | 327.35 | 3.71 | ++ |
| 36 | H | H |  | H | H |  | 341.38 | 3.82 | ++ |

injection. One hour post injection, the mouse brains were perfused with saline, followed by 4% paraformaldehyde (PFA), and removed. The fresh frozen brains were then sectioned. Fluorescently stained myelinated regions such as the cerebellum were then directly examined under a fluorescent microscope. As shown in Figure 5, **32** readily entered the mouse brain and selectively labeled myelinated cerebellum *in situ*.

The nature of **32** binding to myelin was revealed by comparison of **32** staining with immunohistochemical staining for MBP in the cerebellum, caudate putamen, and the temporal cortex regions (Figure 5). In the cerebellum, **32** staining was confined to myelin tracts whereas MBP staining was also observed in the granule cell layers. In the caudate putamen, **32** selectively stained myelin fibers while MBP also stained oligodendrocyte cell soma


dx.doi.org/10.1021/jm101489w |*J. Med. Chem.* 2011, 54, 2331–2340

**Scheme 1. Synthesis of Some Coumarin Derivatives**[a]

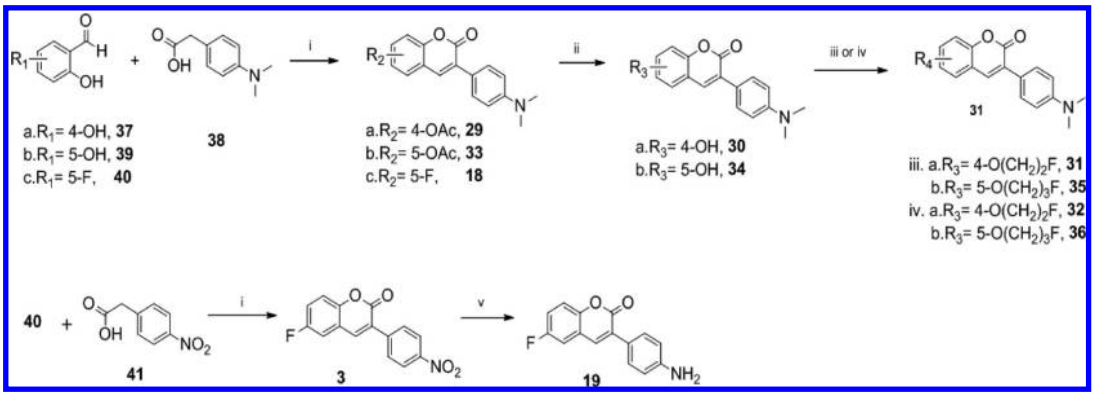


[a] Reagents and conditions: (i) sodium acetate, $Ac_2O$, reflux; (ii) 2 N HCl, MeOH, reflux; (iii) 1-fluoro-2-iodoethane, cerium carbonate, dry acetonitrile, reflux; (iv) 1-fluoro-3-iodopropane, cerium carbonate, dry acetonitrile, reflux; (v) $SnCl_2$, EtOH, reflux.

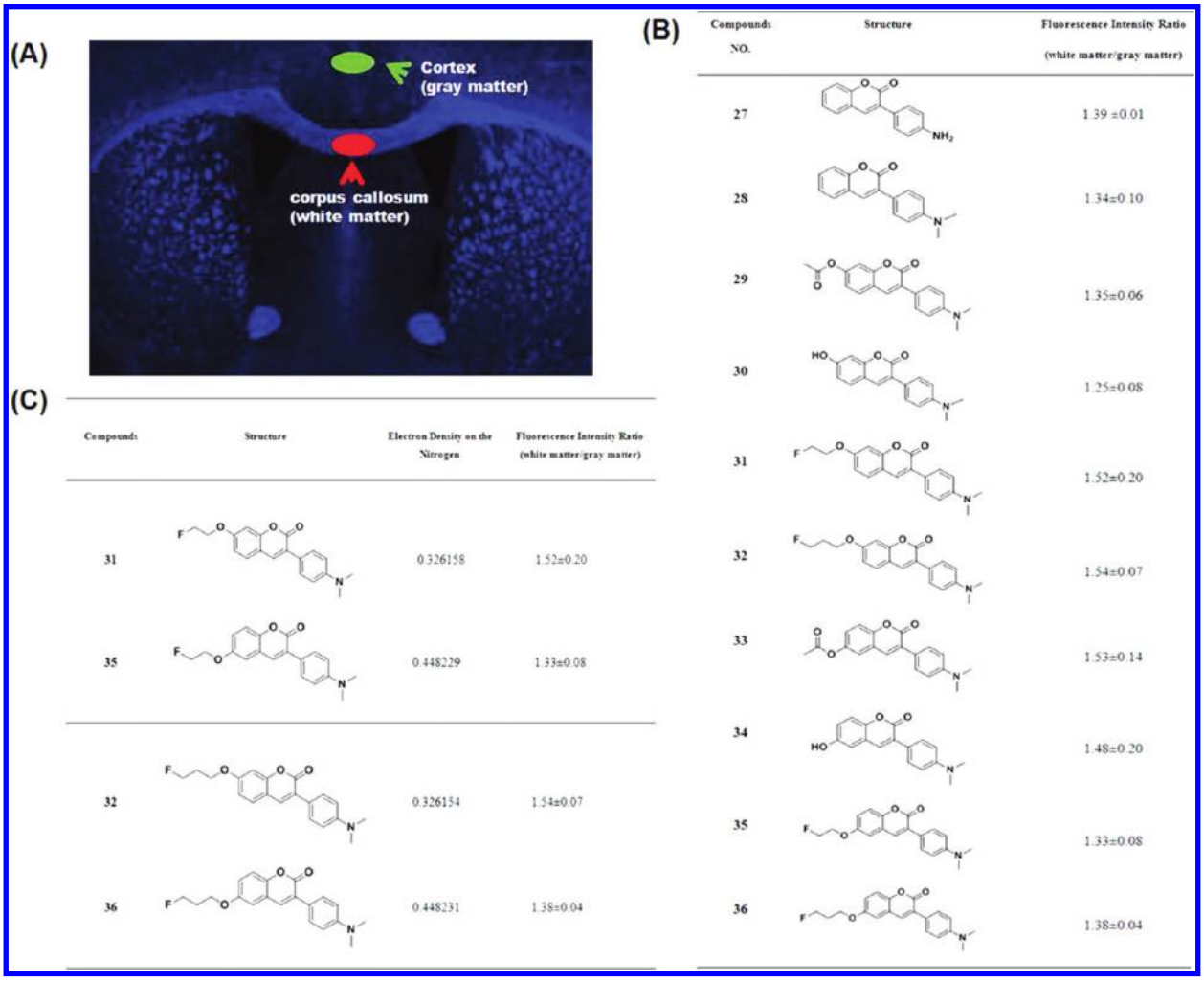


**Figure 2.** (A) Regions of interest (ROI) used for quantification of fluorescent intensity and calculation of binding ratios between the white matter and gray matter. (B) Chemical properties and fluorescence intensity analysis. Log *P* and molecular weight values were calculated by ChemBioOffice 2010, and fluorescence intensity ratios were measured by Image J. Statistical analysis was performed with GraphPad Prism 5, La Jolla, CA (average ± SD, $n = 3$). (C) Comparison of the electron density of nitrogen and fluorescence intensity ratios of **31**, **32**, **35**, and **36**; less electron density of the nitrogen is preferred to enhance the white/gray matter ratio. Therefore, **32** was an ideal probe for further studies. The electron density of nitrogen is calculated using the Hückel method by ChemBioOffice 2010.

and processes. In the temporal cortex, no chemical staining was observed whereas MBP staining revealed the presence of individual myelinated fibers in the subcortical gray matter. These studies suggest that **32** selectively binds to compact myelin.


dx.doi.org/10.1021/jm101489w |*J. Med. Chem.* 2011, 54, 2331–2340

**32 Stains PNS Nerves *In Vivo*.** To examine the ability of **32** to visualize PNS nerves *in vivo*, **32** (40 mg/kg) was administered to wild-type mice via tail vein injection. As shown in Figure 6, 10 min post injection, bright fluorescence was observed in the sciatic nerves exposed under anesthesia. The fluorescence intensities of the nerves were significantly higher than that detected in the surrounding bones or muscles. Thus, **32** could be used intraoperatively to visualize delicate nerves that are prone to damage during surgical procedures in the operating room. These studies indicated that **32** allowed selective visualization of myelinated nerves *in vivo*.

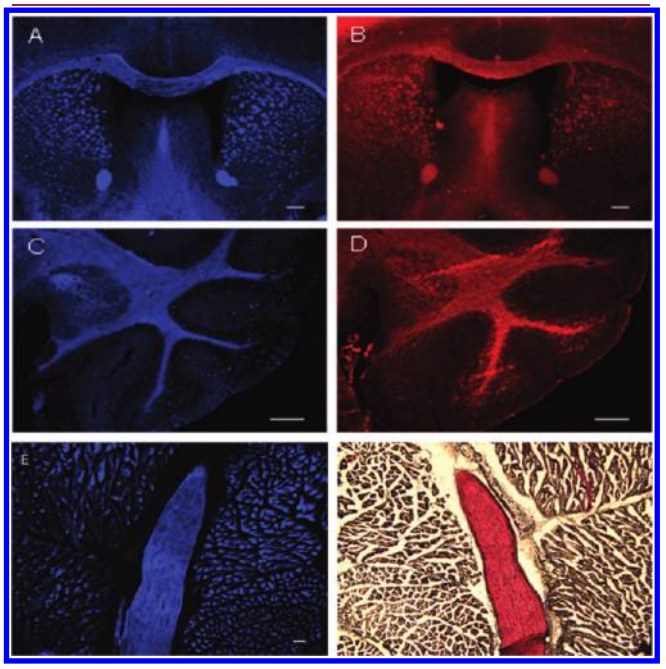


**Figure 3.** *In vitro* **32** staining of the whole mouse brain (A), cerebellum (C), and sciatic nerve (E). For comparison, the same sections were used for MBP staining of the whole mouse brain (B) and cerebellum (D) and for Black-Gold II staining of sciatic nerves (F). Scale bar: A, B = 500 $\mu$m, C, D = 300 $\mu$m, E, F = 100 $\mu$m.

## DISCUSSION

Myelin possesses a unique structure of a highly differentiated multilamellar assembly. It is primarily present in vertebrate species, providing an insulative sheath wrapping around axons to facilitate saltatory conduction in the nervous system.[26] Myelin sheaths are comprised of 70% lipids and 30% proteins, which are distributed according to charge, lipophilicity, and relative molecular weight.[27] Due to its high lipid-to-protein ratio, myelin is considered lipophilic in nature. Thus, SMPs have long been believed to serve as myelin-binding agents that interact with myelin sheaths solely based on lipid-to-lipid interactions with no structural discrimination at the molecular level. Consequently, all molecules that are lipophilic are thought to bind to myelin regardless of their structural differences. Thus, the structural basis of myelin-binding interactions has not been thoroughly examined. Through the structure−activity relationship studies reported herein, we demonstrate that variation of molecular structures leads to very different, often completely opposite myelin-binding properties despite the fact that the lipophilicity of these molecules was found to be very similar. These results suggest that there are specific molecule-to-molecule interactions between SMPs and lipids which determine their binding sensitivity and specificity for myelin.

The precise molecular basis for the selective binding of the coumarin derivatives to myelin remains to be determined but most likely reflects interactions with the unique myelin structure. Myelin sheaths consist of 70% lipid and 30% proteins. In the proteins present in myelin sheaths, the amino acid composition shows a high proportion of nonpolar amino acids, excluding glycine.[28] The binding interaction between the coumarin derivatives and myelin is likely to take place at the hydrophobic sites, which are formed by a focal concentration of nonpolar amino acids, the fatty acids of bound lipids, or some combination of both. The coumarin derivatives could gain access to these sites by virtue of specific interactions with the $NMe_2$ group, since compounds without an $NMe_2$ group showed virtually no affinity for myelin. Because the $NMe_2$ could be retained in the hydrophobic sites, less electron density of the nitrogen is preferred to enhance the lipophilic interactions. Indeed, according to our calculations based on the Hückel method, the electron density of

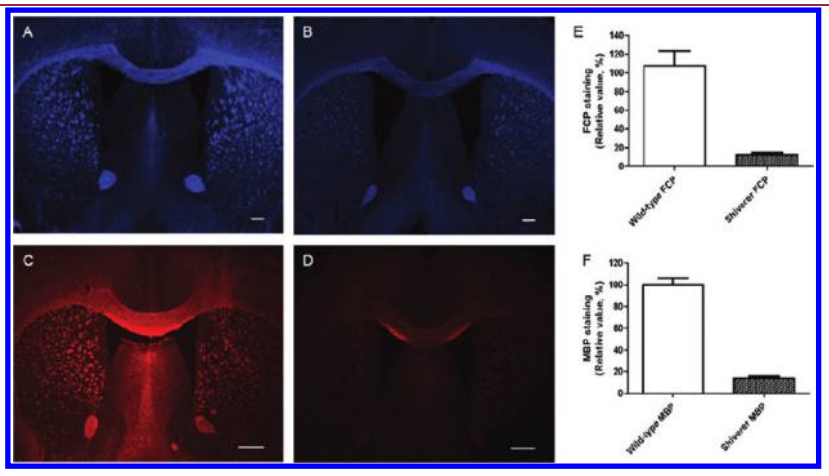


**Figure 4.** Comparison of **32** staining of the wild-type mouse brain (A) and myelin-deficient shiverer mouse brain (B). Staining with anti-MBP of the same brain sections (C, wild-type; D, shiverer) was also conducted for comparison. Fluorescent intensities in the same corpus callosum region following MBP staining and **32** staining were quantified. The data were analyzed using a GraphPad Prism. (E) $P = 0.0005$, $n = 3$, unpaired $t$ test; (F) $P < 0.0001$, $n = 3$, unpaired $t$ test. Scale bar: A, B = 300 $\mu$m, C, D = 500 $\mu$m.


dx.doi.org/10.1021/jm101489w |*J. Med. Chem.* 2011, 54, 2331–2340

the nitrogen in **32** with a fluoropropoxyl group in the 2-position is much lower than that in **36** with a 3-fluoroproxyl group (Figure 2C). The same trend was also observed with the fluoroethoxyl analogues (**31** and **35**). As a result, both **31** and **32** showed a similar binding profile in terms of white/gray matter ratio, which is much higher than that of **35** and **36**.

In addition, we conducted further SAR analysis to address the following important topics:

(1) The necessity of the amino substituent in the active coumarin analogues. As discussed above, myelin sheets consist of 70% lipids and 30% proteins made of a high proportion of nonpolar amino acids. We thus hypothesize that the coumarin derivatives bind to myelin at hydrophobic sites formed by a focal concentration of nonpolar amino acids of myelin proteins and fatty acids of bound lipid. Our SAR studies indicated that the presence of an amino group is critical for active analogues to bind to myelin. However, compounds with a free amino group such as **6**, **7**, **13**, and **14** are too hydrophilic to gain access to the hydrophobic sites. The binding interaction was significantly enhanced when the amino group was dimethylated to increase the lipophilicity. Further SAR analysis shows that the electron density of the nitrogen is also an important factor in the binding interactions.

(2) The importance of a specific range of logPoct in enhancing activity. Lipophilicity is an important property that impacts not only the binding interaction between the coumarin derivatives and myelin but also brain permeability. Previous study has suggested that small molecules with logPoct values ranging from 1.5 to 3 can passively and freely penetrate the blood−brain barrier.[29] Our SAR studies suggest that the logPoct values of active coumarin analogues should be higher than 2.7 in order to exhibit appropriate binding to myelin. This is likely due to the fact that myelin membranes are expected to be more lipophilic than the membranes present in the blood−brain barrier. Thus, we propose that logPoct values between 2.5 and 4.0 are the optimal range for imaging agents to readily enter the brain and selectively bind to myelin. If the lipophilicity is too high, significant nonspecific binding is observed. Thus, with a LogPoct value of 3.82, **32** shows an optimal binding profile and brain permeability.

(3) The significance of hydrogen bonding in interactions between coumarins and the myelin environment. Given the importance of the dimethyl amino group, we proposed that the binding interaction between coumarin derivatives and binding involves, at least in part, hydrogen bonding between the amino group and the amino acids of myelin proteins. Previous studies showed that proteins present in myelin sheaths such as myelin basic protein (MBP) have an overall positive charge at physiological pH because of an excess of lysine and arginine residues.[30] Such residues can act as the hydrogen-bonding donor, and nitrogen in the coumarins acts as an acceptor.

The structure−activity relationship results led us to identify **32** as a lead myelin-imaging agent with promising *in vitro* and *in vivo* binding properties. The fluorescent **32** staining in the CNS was comparable to that of immunohistochemical staining for MBP. High-magnification views of both types of staining in different brain regions suggested that **32** staining was confined to compact myelinated fibers, whereas MBP staining also labeled individual myelinated fibers. **32** fluoresces with relatively high resistance to fading in tissue. This allows us to quantify fluorescence intensity and to correlate changes with myelin content. Using part of the corpus callosum in the white matter and a subcortical region in the gray matter as regions of interest, the ratios of fluorescent intensity between the white matter and gray matter were determined for all myelin-binding compounds (Figure 2B). The ratio of fluorescent intensity can be used as the parameter to examine the binding specificity for myelin in the same brain. As shown in Figure 2B, **32** exhibits the highest ratio of fluorescent intensity between the white matter and gray matter regions.

The binding specificity of **32** was further evaluated by comparison of **32** retention in wild-type brains with a myelin-deficient shiverer mouse model (Figure 4). Compared to

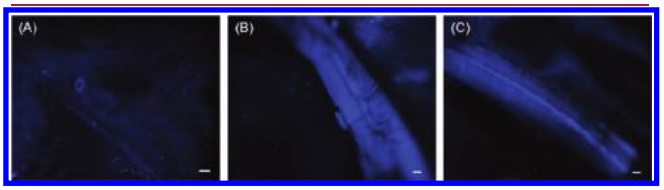


**Figure 6.** *In vivo* visualization of myelinated nerves following injection of **32** in mice. Image A shows the exposure of sciatic nerves in a mouse under anesthesia at 10 min post injection of saline. No fluorescence was observed in sciatic nerves under a dissection fluorescent microscope. At 10 min post injection of 40 mg/kg of **32**, strong fluorescence from **32** was observed in the sciatic nerve (B), which also showed better contrast between the sciatic nerve and surrounding tissues. This remained unchanged after perfusion (C), suggesting that **32** fluorescence was in nerves and not blood vessels. Scale bar: A = 1 mm. B, C = 0.1 mm.

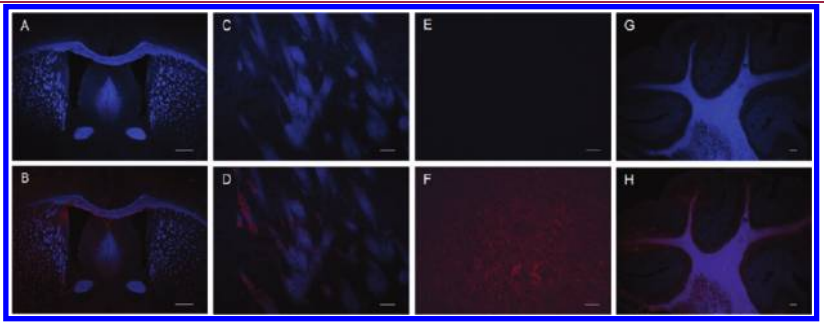


**Figure 5.** *In situ* **32** chemical staining of the brain (A), striatum (C), fibers in cortex (E), and cerebellum (G). **32** did not show binding with small fibers in the cortex. Then the stained sections were double-stained with anti-MBP, and the merged images show the brain (B), striatum (D), fibers in cortex (F), and cerebellum (H). The lack of staining with anti-MBP on the brain, striatum, and cerebellum indicated that **32** can bind MBP on the big bundle of myelin sheaths. Scale bar: A, B = 500 $\mu$m, C, D = 50 $\mu$m, E, F, G, H = 100 $\mu$m.


dx.doi.org/10.1021/jm101489w |*J. Med. Chem.* 2011, 54, 2331–2340

wild-type controls, **32** retention was significantly reduced by 80%, as confirmed by immunohistochemical staining. These studies suggest that **32** is a sensitive and specific myelin-imaging probe that can be selectively retained in the brain proportionally to the degree of myelination.

A unique aspect of this work is the ability of **32** to image myelinated nerves in both the CNS and PNS. To further evaluate the potential of **32** staining of myelinated nerves in the PNS, we examined **32** uptake and retention in sciatic nerves following tail-vein injection. As shown in Figure 6, as early as 10 min after injection of **32**, strong fluorescence appeared in the sciatic nerve, but no significant distribution of **32** was seen in regions surrounding sciatic nerves. Following subsequent perfusion, the sciatic nerves were still readily visualized under the microscope with very good contrast with the surrounding tissues. These studies thus suggest that **32** selectively stained the myelinated nerves in the PNS. Thus, **32** can be used as a fluorescent probe for intraoperative nerve mapping, which is often needed during surgical procedures in which surgeons need to identify myelinated nerves prior to dissecting diseased tissues to preserve functions of normal organs.

A foremost application of **32** may be in PET imaging of demyelination. In our previous studies, we identified some lead compounds that readily entered the brain and selectively localized in the myelinated regions. These findings provide proof-of-the-concept that small-molecule myelin-imaging probes can be developed via direct binding to myelin membranes. However, all of these imaging probes are radiolabeled with C-11. Due to short half-life (20 min), C-11-labeled probes can only be synthesized on site using a dedicated cyclotron and, therefore, are not suitable for remote distribution. Since most clinical facilities do not have an on site cyclotron, use of C-11-labeled imaging agents is limited. In order to enhance the potential of their clinical applications, myelin-imaging agents have to be radiolabeled with fluorine-18, a positron-emitting radionuclide with a half-life of 110 min. F-18-Labeled agents are suitable for regional distribution and thus can be used by PET facilities without an on-site cyclotron. Thus, in future studies, we plan to thoroughly evaluate F-18-labeled **32** for PET studies in a way similar to widely used 2-fluorodeoxyglucose (FDG). Once developed, it can be commercially distributed across the country for routine clinical studies, as is currently done with FDG.

In summary, we have demonstrated that fluorescent coumarin derivatives represented by **32** can be developed as myelin-imaging agents for imaging of myelination in the CNS and nerve mapping in the CNS. In this study, we first show that global lipophilicity is an important factor for brain permeability and binding affinity for myelin. Compounds with a logPoct value between 2.5 and 4 tend to bind to myelin with high affinity. Further SAR analysis indicated that, when lipophilicity is similar, some other physicochemical properties become the determining factors. Because the binding interaction is likely to take place in a hydrophobic environment, the presence of hydrophilic groups such as hydroxyl diminishes the binding affinity. The lower electron density of nitrogen enhances the binding affinity. Through structure−activity studies, we have identified **32**, which readily penetrates the BBB and selectively stained intact myelin sheaths in the brain. **32** can also be used as a fluorescent probe for intraoperative nerve mapping in the PNS. In addition, **32** is capable of radiolabeling with F-18, thus making it a promising candidate as PET radiotracer for routine clinical studies, which will be the primary focus for future investigations.

## EXPERIMENTAL SECTION

**General Remarks.** Compounds **1**, **2**, **4**−**17**, and **20**−**27** are commercially available from Sigma-Aldrich, TCI American, or Alfa Aesar and used without further purification. All NMR spectra were acquired on an Inova 400 NMR equipped with a 5 mm broadband probe. High Resolution ESI-MS were acquired on an ESI-FTICRMS (4.7 T) at the University of Cincinnati Mass Spectrometry Facility. All the intermediates and final product were synthesized in ≥95% purity, as determined by a high pressure liquid chromatography (HPLC) system (Agilent 1100 series, Phenomenex C-18 column, 10 $\mu$m, 250 mm × 10 mm, acetonitrile/$H_2O$ = 80:20 (v/v), flow rate 2.0 mL/min) equipped with a UV detector.

**6-Fluoro-3-(4-nitrophenyl)-2*H*-chromen-2-one (3).** To a round-bottom flask were added **40** (1.4 g, 10.0 mmol), **41** (1.8 g, 10.0 mmol), and sodium acetate (1.6 g, 20.0 mmol), which were then dissolved in $Ac_2O$ (30 mL) and refluxed overnight. After the reaction mixture was cooled to room temperature, the mixture was neutralized with 1 M aqueous NaOH; the solid then was collected, washed with EtOAc, and further purified by recrystallization from EtOAc. The product **3** (2.2 g) was obtained as a yellow solid, yield = 78%. $^1$H NMR (400 MHz, $CDCl_3$): $\delta$ = 8.32 (d, J = 9.2 Hz, 2H), 7.89−7.92 (m, 3H), 7.26−7.42 (m, 3H). HRMS: calcd for $C_{15}H_8FNO_4Na$, 308.0335; found, 308.0333. HPLC purity: 99.95%, retention time: 10.8 min.

**3-(4-(Dimethylamino)phenyl)-6-fluoro-2*H*-chromen-2-one (18).** To a round-bottom flask were added **40** (1.8 g, 12.5 mmol), **38** (2.2 g, 12.5 mmol), and sodium acetate (2.1 g, 25.0 mmol), which were then dissolved in $Ac_2O$ (30 mL) and refluxed overnight. After the reaction mixture was cooled to room temperature, the mixture was neutralized with 1 M aqueous NaOH; the solid then was collected, washed with EtOAc, and further purified by recrystallization from EtOAc. The product **18** (2.3 g) was obtained as a yellow solid, yield = 65.3%. $^1$H NMR (400 MHz, $CDCl_3$): $\delta$ = 7.64−7.68 (m, 3H), 7.31 (t, $J_1 = J_2$ = 4.4 Hz, 1H), 7.28 (d, $J$ = 12.4 Hz, 1H), 6.75−6.79 (m, 2H), 3.02 (s, 6H). HRMS: calcd for $C_{17}H_{14}FNO_2Na$, 306.0906; found, 306.0914. HPLC purity: 99.88%, retention time: 8.7 min.

**3-(4-Aminophenyl)-6-fluoro-2*H*-chromen-2-one (19).** To a round-bottom flask were added **3** (2.0 g, 7.0 mmol) and $SnCl_2$ (8.0 g, 42.0 mmol); ethanol then was added, and the mixture was refluxed overnight. and the ethanol was removed, the residue was neutralized with aqueous 1 M NaOH, and the precipitate was collected. It was then dissolved in a large volume of $CHCl_3$ and filtered, and the filtrate was concentrated to obtain the product **19** (0.63 g) as a yellow solid, yield = 35%. $^1$H NMR (400 MHz, $CDCl_3$): $\delta$ = 7.66 (s, 1H), 7.56 (d, $J$ = 8.8 Hz, 2H), 7.33 (d, $J$ = 4.4 Hz, 1H), 7.30 (d, $J$ = 4.4 Hz, 2H), 6.74 (d, $J$ = 8.4 Hz, 2H), 3.88 (s, 2H). HRMS: calcd for $C_{15}H_{10}FNO_2Na$, 278.0593; found, 278.0593. HPLC purity: 99.95%, retention time: 14.3 min.

**3-(4-(Dimethylamino)phenyl)-2-oxo-2*H*-chromen-7-yl Acetate (29).** To a round-bottom flask were added **37** (2.0 g, 14.5 mmol), **38** (2.6 g, 14.5 mmol), and sodium acetate (2.4 g, 29.0 mmol), which were then dissolved in $Ac_2O$ (30 mL) and refluxed overnight. After the reaction mixture was cooled to room temperature, the mixture was neutralized with 1 M aqueous NaOH; the solid then was collected, washed with EtOAc, and further purified by recrystallization from EtOAc. The product **29** (1.7 g) was collected as a yellow solid, yield = 36.2%. $^1$H NMR (400 MHz, $CDCl_3$): $\delta$ = 7.70 (s, 1H), 7.64 (d, $J$ = 9.2 Hz, 2H), 7.50 (d, $J$ = 8.4 Hz, 1H), 7.11 (d, $J$ = 2.0 Hz, 1H), 7.02−7.05 (m, 1H), 6.76 (d, $J$ = 8.8 Hz, 2H), 3.01 (s, 6H), 2.34 (s, 3H). HRMS: calcd for $C_{19}H_{17}NO_4Na$, 346.1055; found, 346.1047. HPLC purity: 97.21%, retention time: 12.0 min.

**3-(4-(Dimethylamino)phenyl)-7-hydroxy-2*H*-chromen-2-one (30).** To a round-bottom flask was charged **29** (3.0 g, 9.3 mmol), and then 20 mL of MeOH and 10 mL of 2 N HCl were added and refluxed for 4 h. After the reaction mixture was cooled to room

temperature, the mixture was neutralized with 1 M aqueous NaOH; the solid then was collected, washed with EtOAc, and further purified by recrystallization from EtOAc. The product **30** (1.96 g) was collected as a yellow solid, yield = 75%. $^1$H NMR (400 MHz, DMSO-$d_6$): $\delta$ = 7.97 (s, 1H), 7.50−7.55 (m, 3H), 6.68−6.73 (m, 3H), 2.90 (s, 6H). HRMS: calcd for $C_{17}H_{15}NO_3Na$, 304.0950; found, 304.0958. HPLC purity: 99.92%, retention time: 9.0 min.

**3-(4-(Dimethylamino)phenyl)-7-(2-fluoroethoxy)-2*H*-chromen-2-one (31).** To a round-bottom flask were charged **30** (0.5 g, 1.8 mmol), 1-fluoro-2-iodoethane (0.37 g, 2.2 mmol), and cerium carbonate (1.8 g, 3.6 mmol), which were then dissolved in dry acetonitrile (30 mL) and refluxed for 3 h under argon. After the reaction mixture was cooled to room temperature, the solvent was removed and the solid then was suspended in water, filtered, washed with EtOAc, and further purified by recrystallization from EtOAc. The product **31** (0.38 g) was collected as a yellow solid, yield = 64.2%. $^1$H NMR (400 MHz, $CDCl_3$): $\delta$ = 7.62−7.67 (m, 3H), 7.42 (d, $J$ = 8.4 Hz, 1H), 6.84−6.90 (m, 2H), 6.77 (d, $J$ = 8.8 Hz, 2H), 4.73−4.88 (m, 2H), 4.23−4.32 (m, 2H), 3.00 (s, 6H). HRMS: calcd for $C_{19}H_{18}FNO_3Na$, 350.1169; found, 350.1169. HPLC purity: 99.66%, retention time: 12.6 min.

**3-(4-(Dimethylamino)phenyl)-7-(3-fluoropropoxy)-2*H*-chromen-2-one (32).** To a round-bottom flask were charged **30** (0.4 g, 1.4 mmol), 1-fluoro-3-iodopropane (0.32 g, 1.7 mmol), and cerium carbonate (0.91 g, 2.8 mmol), which were then dissolved in dry acetonitrile (30 mL) and refluxed for 3 h under argon. After the reaction mixture was cooled to room temperature, the solvent was removed and then suspended in water, filtered, washed with EtOAc, and further purified by recrystallization from EtOAc. The product **32** (0.32 g) was collected as a yellow solid, yield = 68%. $^1$H NMR (400 MHz, $CDCl_3$): $\delta$ = 8.04 (s, 1H), 7.56−7.64 (m, 3H), 6.93−7.00 (m, 2H), 6.73 (d, $J$ = 8.8 Hz, 2H), 4.52−4.67 (m, 2H), 4.14−4.17 (m, 2H), 2.92 (s, 6H), 2.06−2.16 (m, 2H). HRMS: calcd for $C_{20}H_{20}FNO_3Na$, 364.1325; found, 364.1316. HPLC purity: 95.70%, retention time: 15.8 min.

**3-(4-(Dimethylamino)phenyl)-2-oxo-2*H*-chromen-6-yl acetate (33).** To a round-bottom flask were added **39** (2.5 g, 18.0 mmol), **38** (3.2 g, 18.0 mmol), and sodium acetate (3.0 g, 36.0 mmol), which were then dissolved in $Ac_2O$ (40 mL) and refluxed overnight. After the reaction mixture was cooled to room temperature, the mixture was neutralized with aqueous 1 M NaOH; the solid then was collected, washed with EtOAc, and further purified by recrystallization from EtOAc. The product **33** (4.3 g) was obtained as a yellow solid, yield = 73.1%. $^1$H NMR (400 MHz, $CDCl_3$): $\delta$ = 7.64−7.66 (m, 3H), 7.33 (d, $J$ = 8.8 Hz, 1H), 7.26−7.27 (m, 1H), 7.16−7.19 (m, 1H), 6.76 (d, $J$ = 8.8 Hz, 2H), 3.01 (s, 6H), 2.33 (s, 3H). HRMS: calcd for $C_{17}H_{15}NO_3Na$, 346.1055; found, 346.1053. HPLC purity: 99.56%, retention time: 11.7 min.

**3-(4-(Dimethylamino)phenyl)-6-hydroxy-2*H*-chromen-2-one (34).** To a round-bottom flask was charged **33** (2.9 g, 9.0 mmol), and then 20 mL of MeOH and 10 mL of 2 N HCl were added and refluxed for 4 h. After the reaction mixture was cooled to room temperature, the mixture was neutralized with aqueous 1 M NaOH; the solid then was collected, washed with EtOAc, and further purified by recrystallization from EtOAc. The product **34** (1.8 g) was obtained as a yellow solid, yield = 70.6%. $^1$H NMR (400 MHz, $CDCl_3$): $\delta$ = 7.63−7.67 (m, 3H), 7.20−7.26 (m, 1H), 6.93−6.97 (m, 2H), 6.77 (d, $J$ = 9.2 Hz, 2H), 4.80 (s, 1H), 3.01 (s, 6H). HRMS: calcd for $C_{17}H_{15}NO_3Na$, 304.0950; found, 304.0958. HPLC purity: 97.70%, retention time: 8.7 min.

**3-(4-(Dimethylamino)phenyl)-6-(2-fluoroethoxy)-2*H*-chromen-2-one (35).** To a round-bottom flask were charged **34** (0.56 g, 2.0 mmol), 1-fluoro-2-iodoethane (0.40 g, 2.4 mmol), and cerium carbonate (2.0 g, 4.0 mmol), which were then dissolved in dry acetonitrile (30 mL) and refluxed for 3 h under argon. After the reaction mixture was cooled to room temperature, the solvent was removed and the solid then was suspended in water, filtered, washed with EtOAc, and further purified by recrystallization from EtOAc. The product **35** (0.38 g) was obtained as a yellow solid, yield = 58.4%. $^1$H NMR (400 MHz, $CDCl_3$): $\delta$ = 7.67−7.67 (m, 3H), 7.27 (d, $J$ = 9.2 Hz, 1H), 7.06−7.09 (m, 1H), 6.97 (d, $J$ = 2.8 Hz, 1H), 6.76 (d, $J$ = 8.8 Hz, 2H), 4.72−4.85 (m, 2H), 4.21−4.30 (m, 2H), 3.01 (s, 6H). HRMS: calcd for $C_{19}H_{18}NO_4$ ($M + H^+$), 328.1349; found, 328.1357. HPLC purity: 98.93%, retention time: 12.1 min.

**3-(4-(Dimethylamino)phenyl)-6-(3-fluoropropoxy)-2*H*-chromen-2-one (36).** To a round-bottom flask were charged **34** (0.42 g, 1.5 mmol), 1-fluoro-3-iodopropane (0.34 g, 1.8 mmol), and cerium carbonate (0.98 g, 3.0 mmol), which were then dissolved in dry acetonitrile (30 mL) and refluxed for 3 h under argon. After the reaction mixture was cooled to room temperature, the solvent was removed and then suspended in water, filtered, washed with EtOAc, and further purified by recrystallization from EtOAc. The product **36** (0.30 g) was obtained as a yellow solid, yield = 59.1%. $^1$H NMR (400 MHz, $CDCl_3$): $\delta$ = 7.64−7.87 (m, 3H), 7.24−7.27 (m, 1H), 6.96−7.05 (m, 2H), 6.97 (d, $J$ = 2.8 Hz, 1H), 4.60−4.74 (m, 2H), 4.13 (t, $J_1 = J_2$ = 6.0 Hz, 2H), 3.01 (s, 6H), 2.15−2.25 (m, 2H). HRMS: calcd for $C_{20}H_{21}FNO_3$ ($M + H^+$), 342.1505; found, 342.1514. HPLC purity: 98.88%, retention time: 14.9 min.

## ■ ANIMAL PREPARATION AND STUDIES

**Animals.** All animal experiments were performed in accordance with the guidelines approved by the Institutional Animal Care and Use Committee of Case Western Reserve University (Protocol 2010-0007). The animals were subjected to minimal stress during tail vein injections. The 8-week old C57BL/6 mice and C3Fe.SWV-Mbp$^{shi}$/J shiverer mice were obtained from The Jackson Laboratory, Bar Harbor, MN.

**Euthanasia.** Mice were deeply anesthetized with isoflurane and perfused via the ascending aorta with 1xPBS followed by 4% paraformaldehyde in 1xPBS. Brains and sciatic nerves were removed and incubated for 24 h in 4% paraformaldehyde at 4 °C.

**Tissue Processing.** Brain and sciatic nerve tissue were rinsed in 1xPBS. After treatment with 4% PFA overnight, the tissues were incubated in 30% sucrose until submerged. For preparation of fresh frozen sections, the cryoprotected tissues were first frozen in OCT on dry ice before axial sectioning (20 $\mu$m) with a cryostat at −20 °C. Tissue sections from the midline of the brain containing the whole corpus callosum were selected for staining. Stained sections were covered with fluorescence mounting medium (Vectashield, Vector Laboratories) and stored at 4 °C for future analysis.

**Chemical staining.** Fresh frozen sections with 20 $\mu$m in thickness were incubated in 0.1% Triton-100 in 1xPBS for 10 min and then incubated in a solution of compounds (100 $\mu$M) in 10%DMSO/$H_2O$ for 30 min at room temperature. The fresh frozen sections were then washed three times for 5 min each with PBS before coverslipping with fluorescence mounting medium. Images of the stained mouse brain sections were acquired on a Leica DMI5000 inverted microscope (BP470/40 nm filter).

**Immunohistochemistry.** Fresh frozen sections were rinsed in 3% normal goat serum in 0.1% TritonX-100/1xPBS three times for 5 min each and washed with 1xPBS three times for 5 min each. The sections then were immunostained overnight at 4 °C with purified mouse antibody monoclonal (Covance, Inc., Princeton, NJ) 1:500 dilution in 3% normal goat serum in 1xPBS. Sections were incubated for 1 h at room temperature in Cy3 AffiniPure Goat Anti-Mouse IgG (H+L) (Jackson ImmunoResearch Laboratories, Inc. West Grove, PA) and rinsed in PBS three times for 5 min each. Images of the stained mouse brain sections were

acquired on a Leica DMI5000 inverted microscope (BP 645/75 filter).

**Black-Gold II Staining.** A 0.3% solution of Black-Gold II was made by adding 150 mg of Black-Gold II to 50 mL of 0.9% NaCl. The solution was fully equilibrated to 60 °C in a water bath. The slide mounted tissue sections were transferred to this warm Black Gold II impregnating solution in the water bath, and the staining was visually monitored. Images of the stained mouse brain sections were acquired on a Leica DMI5000 inverted microscope (bright field).

**Quantification and Statistical Analysis.** Image *J* software (http://rsb.info.nih.gov/ij/) was used to quantify pixel intensities values. The corpus callosum between the midline and below the apex of the cingulum was defined as ROI. The density of myelin in the corpus callosum of wild-type mice was given the arbitrary value of 100, and the density of myelin in shiverer mice was determined as a percentage of wild-type mice. The data were analyzed using the GraphPad Prism, GraphPad Software, La Jolla, CA, with a nonpaired Student's *t* test.

***In Situ* Tissue Staining of Normal Control Mice Brain Section.** Under anesthesia, wild-type mice were injected with **32** (40 mg/kg) via the tail vein, and the mice were then perfused transcardially with saline followed by 4% PFA in 1xPBS. Brain tissues were then removed, postfixed by immersion in 4% PFA overnight, dehydrated in 30% sucrose solution, cryostat sectioned at 20 $\mu$m on a microtome, and mounted on superfrost slides (Fisher Scientific). For the direct detection, the sections were coverslipped with fluoromounce mounting media (Vector Laboratories, Burlingame, CA). Images of the stained mouse brain sections were acquired on a Leica DMI5000 inverted microscope (BP470/40 nm filter). For the immunohistochemical costaining, the sections were stained with anti-MBP antibody following the procedure described above.

***In Vivo* Visualization of PNS Nerves.** Eight-week-old C57BL/6 black mice were administered via tail vein injection a dose of 40 mg/kg **32** using saline as the vehicle. Ten minutes post injection, the mice were deeply anesthetized with isoflurane. Sciatic nerves in the leg regions were then surgically exposed and imaged use a Leica M216FA dissection fluorescent microscope (LP 590 filter). After imaging, the mice were perfused as described above, and then the sciatic nerves were imaged again.

## ■ ASSOCIATED CONTENT

**Supporting Information.** NMR, HRMS, and HPLC data. This material is available free of charge via the Internet at http://pubs.acs.org.

## ■ AUTHOR INFORMATION

### Corresponding Author

*Telephone: 216 844 3288. Fax: 216 844 8062. E-mail: yanming.wang@case.edu.

## ■ ACKNOWLEDGMENT

We gratefully acknowledge the financial support of this project by grants from the NIH/NINDS (R01 NS061837), the Department of Defense (MS090082), and the National Multiple Sclerosis Society. We thank Dr. James Basilion for letting us use his dissection microscope. We also thank Dr. George Bakale for his assistance with preparation of the manuscript.

## ■ ABBREVIATIONS USED

CNS, central nervous system; PNS, peripheral nervous system; MS, multiple sclerosis; MRI, magnetic resonance imaging; SMP, small-molecule probes; PET, positron emission tomography; BMB, (*E*,*E*)-1,4-bis(*p*-aminostyryl)-2-methoxybenzene; BDB, (*E*,*E*)-1,4-bis-(4′-aminostyryl)-2,5-dimethoxybenzene; DAS, 4,4′-diamino-*trans*-stilbene; CMC, 3-(4-aminophenyl)-2H-chromen-2-one; DBT, 3,3′-diethylthiatricarbocyanine iodide; FIC, fluorinated imaging compound; ROI, regions of interest; FDG, 2-fluorodeoxyglucose

## ■ REFERENCES

(1) Compston, A.; Coles, A. Multiple sclerosis. *Lancet* **2002**, *359*, 1221–1231.

(2) Compston, A.; Coles, A. Multiple sclerosis. *Lancet* **2008**, *372*, 1502–1517.

(3) Rosati, G. The prevalence of multiple sclerosis in the world: an update. *Neurol. Sci.* **2001**, *22*, 117–139.

(4) Ascherio, A.; Munger, K. L. Environmental risk factors for multiple sclerosis. Part I: the role of infection. *Ann. Neurol.* **2007**, *61*, 288–299.

(5) Lublin, F. D.; Reingold, S. C. Defining the clinical course of multiple sclerosis: results of an international survey. National Multiple Sclerosis Society (USA) Advisory Committee on Clinical Trials of New Agents in Multiple Sclerosis. *Neurology* **1996**, *46*, 907–911.

(6) Liu, L.; Darnall, L.; Taofang, H.; Choi, K.; Lane, T. E.; Ransohoff, R. M. Myelin Repair Is Accelerated by Inactivating CXCR2 on Non-hematopoietic Cells. *J. Neurosci.* **2010**, *30*, 9074–9083.

(7) Piaton, G.; Gould, R. M.; Lubetzki, C. Axon-oligodendrocyte interactions during developmental myelination, demyelination and repair. *J. Neurochem.* **2010**, *114*, 1243–1260.

(8) Miller, R. H.; Sha, M. Dissecting demyelination. *Nat. Neurosci.* **2007**, *10*, 1351–1354.

(9) Matsas, R.; Lavdas, A. A.; Papastefanaki, F.; Thomaidou, D. Schwann Cell Transplantation for CNS Repair. *Curr. Med. Chem.* **2008**, *15*, 151–160.

(10) Peru, R. L.; Mandrycky, N.; Nait-Oumesmar, B.; Lu, Q. R. Paving the Axonal Highway: From Stem Cells to Myelin Repair. *Stem Cell Rev.* **2008**, *4*, 304–318.

(11) Mozafari, S.; Sherafat, M. A.; Javan, M.; Mirnajafi-Zadeh, J.; Tiraihi, T. Visual evoked potentials and MBP gene expression imply endogenous myelin repair in adult rat optic nerve and chiasm following local lysolecithin induced demyelination. *Brain Res.* **2010**, *1351*, 50–56.

(12) Nait-Oumesmar, B.; Picard-Riéra, N.; Kerninon, C.; Baron-Van Evercooren, A. The role of SVZ-derived neural precursors in demyelinating diseases: From animal models to multiple sclerosis. *J. Neurol. Sci.* **2008**, *265*, 26–31.

(13) Franklin, R. J.; Hinks, G. L. Understanding CNS remyelination: clues from developmental and regeneration biology. *J. Neurosci. Res.* **1999**, *58*, 207–213.

(14) Stangel, M.; Hartung, H. P. Remyelinating strategies for the treatment of multiple sclerosis. *Prog. Neurobiol.* **2002**, *68*, 361–376.

(15) Polman, C. H.; Reingold, S. C.; Edan, G.; Filippi, M.; Hartung, H. P.; Kappos, L.; Lublin, F. D.; Metz, L. M.; McFarland, H. F.; O'Connor, P. W.; Sandberg-Wollheim, M.; Thompson, A. J.; Weinshenker, B. G.; Wolinsky, J. S. Diagnostic criteria for multiple sclerosis: 2005 revisions to the "McDonald Criteria. *Ann. Neurol.* **2005**, *58*, 840–846.

(16) Molyneux, P. D.; Barker, G. J.; Barkhof, F.; Beckmann, K.; Dahlke, F.; Filippi, M.; Ghazi, M.; Hahn, D.; MacManus, D.; Polman, C.; Pozzilli, C.; Kappos, L.; Thompson, A. J.; Wagner, K.; Yousry, T.; Miller, D. H. Clinical-MRI correlations in a European trial of interferon beta-1b in secondary progressive MS. *Neurology* **2001**, *57*, 2191–2197.

(17) Stankoff, B.; Wang, Y. M.; Bottlaender, M.; Aigrot, M. S.; Dolle, F.; Wu, C.; Feinstein, D.; Huang, G. F.; Semah, F.; Mathis, C. A.; Klunk, W.; Gould, R. M.; Lubetzki, C.; Zalc, B. Imaging of CNS myelin by

positron emission tomography. *Proc. Natl. Acad. Sci. USA* **2006**, *103*, 9304–9309.

(18) Wu, C.; Tian, D.; Feng, Y.; Polak, P.; Wei, J.; Sharp, A.; Stankoff, B.; Lubetzki, C.; Zalc, B.; Mufson, E. J.; Gould, R. M.; Feinstein, D. L.; Wang, Y. A novel fluorescent probe that is brain permeable and selectively binds to myelin. *J. Histochem. Cytochem.* **2006**, *54*, 997–1004.

(19) Wu, C.; Wei, J.; Tian, D.; Feng, Y.; Miller, R. H.; Wang, Y. Molecular probes for imaging myelinated white matter in CNS. *J. Med. Chem.* **2008**, *51*, 6682–6688.

(20) Caprariello, A. V.; Somoza, E.; Zhu, W.; Wang, C.; Miller, R. H. In vivo quantification of myelin changes in the vertebrate nervous system. *J. Neurosci.* **2009**, *29*, 14663–14669.

(21) Wang, C.; Wu, C.; Zhu, J.; Popescu, D. C.; Macklin, W.; Miller, R. H.; Wang, Y. Longitudinal Near Infrared Imaging of Myelination. *J. Neurosci.* **2010**, in press. DOI: 10.1523/JNEUROSCI.2698-10.2010.

(22) Wu, C.; Wang, C.; Popescu, D. C.; Zhu, W.; Somoza, E.; Zhu, J.; Flask, C.; Miller, R. H.; Macklin, W.; Wang, Y. A novel PET marker for *in vivo* quantification of myelination. *Bioorg. Med. Chem.* **2010**, *18*, 8592–8599.

(23) Wang, C.; Popescu, D. C.; Wu, C.; Zhu, J.; Macklin, W.; Wang, Y. In Situ fluorescence Imaging of Myelination. *J. Histochem. Cytochem.* **2010**, *58*, 611–621.

(24) Casley-Smith, J. R. Benzopyrones in the treatment of lymphedema. *Int. Angiol.* **1999**, *18*, 41976–41990.

(25) Luszczki, J. J.; Andres-Mach, M.; Cisowski, W.; Mazol, I.; Glowniak, K.; Czuczwar, S. J. Osthole suppresses seizures in the mouse maximal electroshock seizure model. *Eur. J. Pharmacol.* **2009**, *607*, 107–109.

(26) Waxman, S. G.; Bangalore, L. Electrophysiologic consequences of myelination. In Lazzarini, R. A., Ed.; *Myelin biology and disorders*; Elsevier: London, 2004; Vol. 1, pp 117−143.

(27) Podbielska, M.; Hogan, E. L. Molecular and immunogenic features of myelin lipids: incitants or modulators of multiple sclerosis? *Multiple Sclerosis* **2009**, *15*, 1011–1029

(28) Clasen, R. A.; Simon, R. G.; Scott, R.; Pandolfi, S.; Laihg, I.; Lesak, A. The staining of the myelin sheath byluxol dye techniques. *J. Neuropathol. Exp. Neurol.* **1973**, *32*, 271–283.

(29) Dischino, D. D.; Welch, M. J.; Kilbourn, A.; Raichle, M. E. Relationship between lipophilicity and brain extraction of C-11-labeled radiopharmaceuticals. *J. Nucl. Med.* **1983**, *24*, 1030–1038.

(30) Hu, Y.; Doudevski, I.; Wood, D.; Moscarello, M.; Husted, C.; Genain, C.; Zasadzinski, J. A.; Israelachvili, J. Synergistic interactions of lipids and myelin basic protein. *Proc. Natl. Acad. Sci. USA* **2004**, *101*, 13466–1347.